applied sciences

MDPI

Article

Calculation Method of Rotational Constraint Stiffness for a New Tower-Pier Connected System

Yajun Zhang [1,2], Yu Zhao [2], Yongjun Zhou [2] and Xia Yang [3,*]

[1] Ningxia Communications Construction Co., Ltd., Yinchuan 750004, China
[2] School of Highway, Chang'an University, Xi'an 710064, China
[3] College of Civil Engineering, Tongji University, Shanghai 200092, China
* Correspondence: xiay@tongji.edu.cn

Abstract: The universal hinge support (UHS) is a new connection system for the tower and pier of a single-tower cable-stayed bridge (STCSB), which could conform the multi-direction rotation of the tower and release the bending moment at the bottom of the tower in all directions. However, UHS is not an ideal hinge in practical projects, and the rotational constraint stiffness (RCS) of UHS is constantly changed with construction. In order to determine the RCS of UHS in situ, parametric analysis was performed by establishing a theoretical mechanical model of plane rotation and a refined solid finite element (FE) model of UHS. The slope of the linear rising segment of the load–displacement curve obtained from the numerical simulation was considered as the RCS of the UHS. The relationships between RCS and the vertical force, geometric parameters, and material parameters were established, and then the calculation formula of RCS was further proposed. To verify the accuracy of the proposed formula, a case study for a real bridge was conducted in this paper. The results show that the error of the tower rotation displacement can be reduced by about 90% using the proposed method compared with the conventional method, which regards the hinge as an ideal one, and the precision is greatly improved. This study has enormous potential to quickly determinate the RCS of UHS in practical applications, and plays a great promotion role in enriching the structural system of cable-stayed bridges.

Keywords: single-tower cable-stayed bridge (STCSB); tower bottom support; universal hinge support (UHS); rotational constraint stiffness (RCS); numerical simulation

Citation: Zhang, Y.; Zhao, Y.; Zhou, Y.; Yang, X. Calculation Method of Rotational Constraint Stiffness for a New Tower-Pier Connected System. *Appl. Sci.* **2022**, *12*, 11221. https://doi.org/10.3390/app122111221

Academic Editors: Tong Guo and Zhongxiang Liu

Received: 4 October 2022
Accepted: 1 November 2022
Published: 5 November 2022

1. Introduction

A cable-stayed bridge is formed by three main structural elements: deck, towers, and cable-stays. According to the difference in the connection patterns between the tower, main beam, and pier, the cable-stayed bridge can be divided into four systems: a floating system, semi-floating system, tower-beam consolidation system, and rigid frame system [1–3]. As bridge engineers pay more and more attention to bridge aesthetics, many special-shaped cable-stayed bridges have been designed and built, such as Australia's Batman Bridge, Spain's Alamillo Bridge, China's Hunan Hongshanmiao Bridge, and so on [4–11]. These are mostly irrational in mechanics due to their strange appearance, while they are generally regarded as landmarks of the city because of their special appearance. For these bridges, the pier and tower become whole through rigid connection. Huge internal forces will be generated at the root of the tower under loads [12], which need to be resisted by increasing the size of the cross-section of the tower. However, the increased sizes will lead to an increased cost for the project.

Engineers have tried to solve the above problem through structural optimization [13]. For the Tianjin Tuanbo New Bridge [14], built in China in 2011, and the Shanghai Wenzaobang Bridge [15,16], built in China in 2014, the structural designs were optimized by changing the structural system, and the one-way hinge support was used to connect the

bridge tower and pier in the longitudinal direction of the bridge. So, the bridge tower is allowed to rotate along the longitudinal direction of the bridge, which releases the huge bending moment at the root of the bridge tower, makes the force in the bridge more reasonable, and the tower becomes lighter and more shapely. These two cases provide new ideas to solve the problem of unreasonable force in the STCSB.

However, for a special-shaped cable-stayed bridge with asymmetry in both the transverse and longitudinal directions, the root of the tower will suffer a large bending moment in both the transverse and longitudinal directions under loads [12]. The one-way hinge at the tower bottom cannot solve the problem of the bending moments generated in the transverse direction. Therefore, the Sanya Landscape Bridge innovatively adopts universal hinge support (UHS) to replace the traditional connection mode between the bridge tower and pier [17,18]. UHS is composed of a top plate and bottom basin. The huge bending moment at the root of the tower can be released through the rotation of the top plate, and this rotation behavior is similar to a gyrostat [19,20]. The mechanical properties of the bridge structure using UHS are improved, and the structural safeties of the steel bridge tower and concrete pier are greatly upgraded. In addition, the bridge tower size can have more design space, which also creates more possibilities in the structural form and aesthetics. This design is an innovation in the connection between the tower and the pier of the cable-stayed bridge, and it is also a new connection pattern between different materials, that is, a steel tower and concrete pier.

In order to simplify the calculation, the boundary conditions are usually idealized when the bridge structure is designed and calculated. However, in practical applications, considering the great difficulty when replacing the UHS at the tower bottom during service, in order to synchronize the service life of the UHS with that of the bridge, rubber or ultra-high molecular weight polyethylene slide plates are not used between the top plate and the bottom basin, which eliminates the impact of material aging on the durability of the UHS [21–24] and makes it meet the requirement of not being replaced within the design service life. Unfortunately, not using slide plates will lead to greater friction between the top plate and the bottom basin, which is a non-ignorant factor for in structural safety calculations. The previous studies demonstrate that the boundary conditions have a great impact on the structure performance [25,26]. Therefore, UHS cannot be considered as an ideal hinged boundary condition in structural calculations, and the real boundary parameters of UHS need to be known.

The friction behaviors in engineering applications are mostly calculated through a numerical method [27–29]. The structural response can be accurately obtained by establishing a multi-scale finite element (FE) model [30–35]. Mohammadreza Salehi et al. also tried to use artificial neural networks to identify structural boundary conditions [36]. In general, the construction parameters are determined by repeatedly updating the relevant parameters according to the structural state of the construction process, which generally need so much time for each iteration of the multi-scale modeling calculation method, that it is unacceptable for large-scale bridge building construction. In addition, the method using artificial neural networks could not directly obtain the stiffness parameters of UHS. To solve these problems, this paper proposed a calculation model to quickly and accurately determine the rotational constraint stiffness (RCS) of UHS to optimize the structural calculation procedure, so that engineers could easily obtain the true response of the structure of UHS using the model.

The proposed calculation model uses the finite element method and theoretical analysis to study the boundary parameters of UHS. At first, a theoretical mechanical model of the plane rotation of UHS was established to compute the critical torque. Secondly, the refined FE model of the UHS was built and its effectiveness was verified by the above theoretical model, and we further established the RCS calculation model of UHS by analyzing the influence of vertical force, the friction coefficient between the components, and the geometry parameters on RCS. This study can provide reference for the design and construction

of practical projects using UHS, and shows promise for the application of special-shaped bridge structures.

2. The Plane Rotation Model of UHS

UHS is mainly composed of a bottom basin and top plate. The top plate is connected to the bridge tower by bolts and shear tenons. The connection between the bottom basin and the concrete pier is performed by high-strength bolts, and the concrete is then poured to seal the anchor. The geometric model of the UHS is shown in Figure 1.

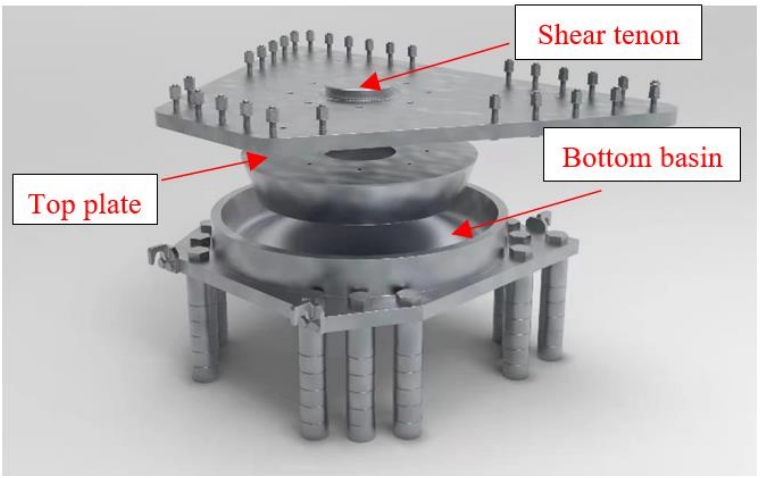

Figure 1. Geometric model of UHS.

Most research on bridge bearings mainly focuses on the vertical plane rotation of the bearings [37–40], while only few studies have been performed to explore the properties of the horizontal-plane rotation, as Figure 2 shows.

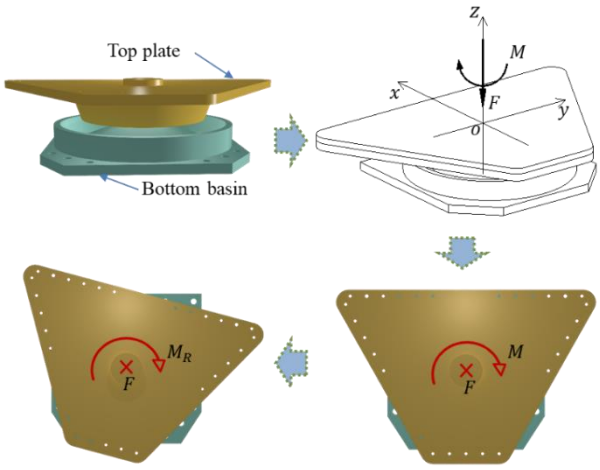

Figure 2. The rotation model of the UHS.

The top plate and the bottom basin are in frictional contact under a vertical force F. When the torque M transmitted by the bridge tower to the UHS increases to the critical torque M_R, the friction behavior between the top plate and the bottom basin has converted from static friction to dynamic friction. The top plate rotates around the UHS z-axis due to the rigid connections, and is adopted between the bottom basin and the concrete pier. During the process of rotation, the critical torque will vary with the variation in the vertical force F. In addition, the critical torque also depends on the friction coefficient and the size of the UHS.

The stress decomposition of UHS is shown in Figure 3, where q_0 is the uniform distributed force at the top plate (that is, the equivalent uniform load of F) and q is the uniform force transmitted from the top plate to the bottom basin. R_0 is the spherical radius of UHS, R_1 is the radius of the vertical projection surface of the arc-contact surface, and R_2 is the radius of the arc-contact surface, $R_2 = R_0 \times \theta \times \frac{\pi}{180^\circ}$.

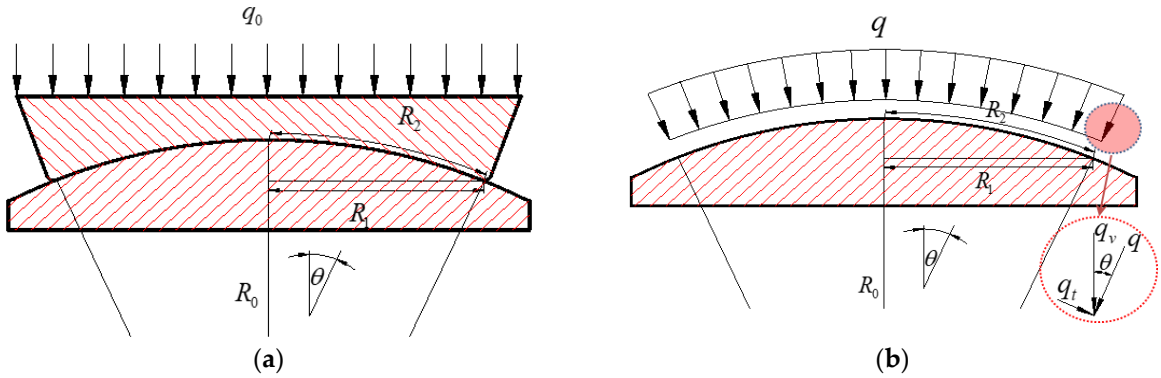

Figure 3. Force transmission diagram: (**a**) the force transmitted from the tower to the top plate; (**b**) the force transferred from the top plate to the bottom basin.

The differential idea is used to solve the critical torque of the UHS. The contact surface between the top plate and the bottom basin is unfolded, as shown in Figure 4, where ds is the area of the micro-ring with radius r and $ds = 2\pi r dr$.

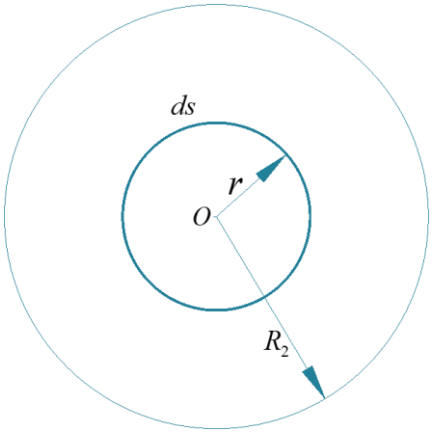

Figure 4. Unfolding plane of the contact surface between the top plate and bottom basin of UHS.

Make the following assumptions in the calculation:

(1) The pressure on the contact surface is evenly distributed along the surface.
(2) Both the top plate and the bottom basin are rigid bodies.

According to Figures 3 and 4, the vertical uniform distribution force of the peak point of the arc surface is $q_v = q$ and the vertical uniform distribution force of the lowest point of the arc surface is $q_v = \frac{q}{cos\theta}$. For the convenience of calculation, the vertical uniform distribution force of any point on the arc surface is approximated as $q_v = \left(q + \frac{q}{cos\theta}\right)/2$, then the uniform distribution force on the surface is as follows:

$$q = 2q_v / \left(1 + \frac{1}{\cos\theta}\right) \tag{1}$$

The pressure of the micro-ring in Figure 4 can be obtained according to Equation (1):

$$dF = q\mathrm{d}s = 2\pi q r \mathrm{d}r \tag{2}$$

The friction force df on the micro-ring can be obtained according to Coulomb's friction formula ($f = \mu \times F$) and Equation (2):

$$\mathrm{d}f = \mu dF = 2\pi\mu q r \mathrm{d}r \tag{3}$$

Then, the torque of the friction force on the micro-ring to the center of the arc-contact surface is as follows:

$$\mathrm{d}M = df \times r = 2\pi\mu q r^2 \mathrm{d}r \tag{4}$$

The torque generated by the total friction force on the arc-contact surface to the center of the circle can be obtained by integrating Equation (4):

$$M_R = \int_0^{R_2} \mathrm{d}M = \int_0^{R_2} 2\pi\mu q r^2 \mathrm{d}r = \frac{2}{3}\pi\mu q {R_2}^3 \tag{5}$$

Substituting Equation $q_v = F/\left(\pi {R_2}^2\right)$ into Equation (1):

$$q = \frac{2F}{\pi {R_2}^2} / \left(1 + \frac{1}{\cos\theta}\right) \tag{6}$$

Substituting Equation (6) into Equation (5), the critical torque can be obtained:

$$M_R = \frac{2}{3}\mu \frac{2F}{1 + \sec\theta} R_2 \tag{7}$$

3. RCS Calculation Model of UHS

3.1. Finite Element Model of UHS

1. Material parameters

The top plate and bottom basin of UHS are made of ZG20MnMo low alloy steel with an elastic modulus of 196 GPa and a Poisson's ratio of 0.3.

2. Mesh partition

To ensure the calculational accuracy, the FE model of UHS was simplified to reduce the computational costs, and the simplified model is shown in Figure 5. The element type of the component of UHS adopts C3D10 in this model.

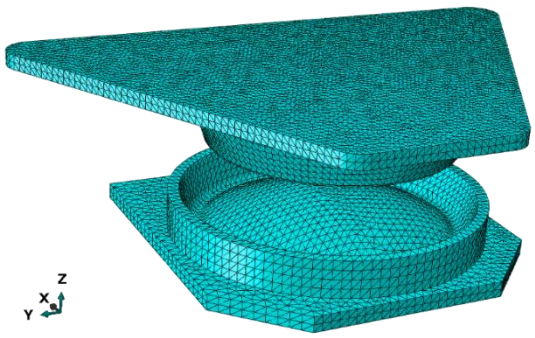

Figure 5. Numerical model of UHS.

3. Boundary conditions and loads

The bottom of the bottom basin is completely fixed by being "pinned", and the upper surface of the top plate is coupled with the reference point "RP" to constrain its translational displacement in the x-axis and y-axis directions through "coupling". In order to ensure a good convergence of the model, torque loading is replaced by angular displacement loading, and the angular displacement is loaded by a step of 3° (0.05 rad) around the z-axis.

4. Definition of interaction

The normal behavior between the bottom basin and the top plate adopts the "hard contact" model, and the tangential behavior adopts the "penalty friction".

3.2. Parametric Analysis of RCS

This part studies the influence of the vertical force F, central angle θ, radius of curvature R_0, and friction coefficient μ on RCS of the UHS.

3.2.1. Influence of Vertical Force on RCS

1. Critical torque analysis

When the radius of curvature is R_0 = 1.5 m, the friction coefficient of contact surface is μ = 0.15 (for steel and steel) and the central angle is θ = 23.5°, the vertical force is loaded by six cases according to 10 MN, 20 MN, 30 MN, 40 MN, 50 MN, and 60 MN for the calculation of the FE model, and the the load–displacement curve of each case is obtained, as shown in Figure 6.

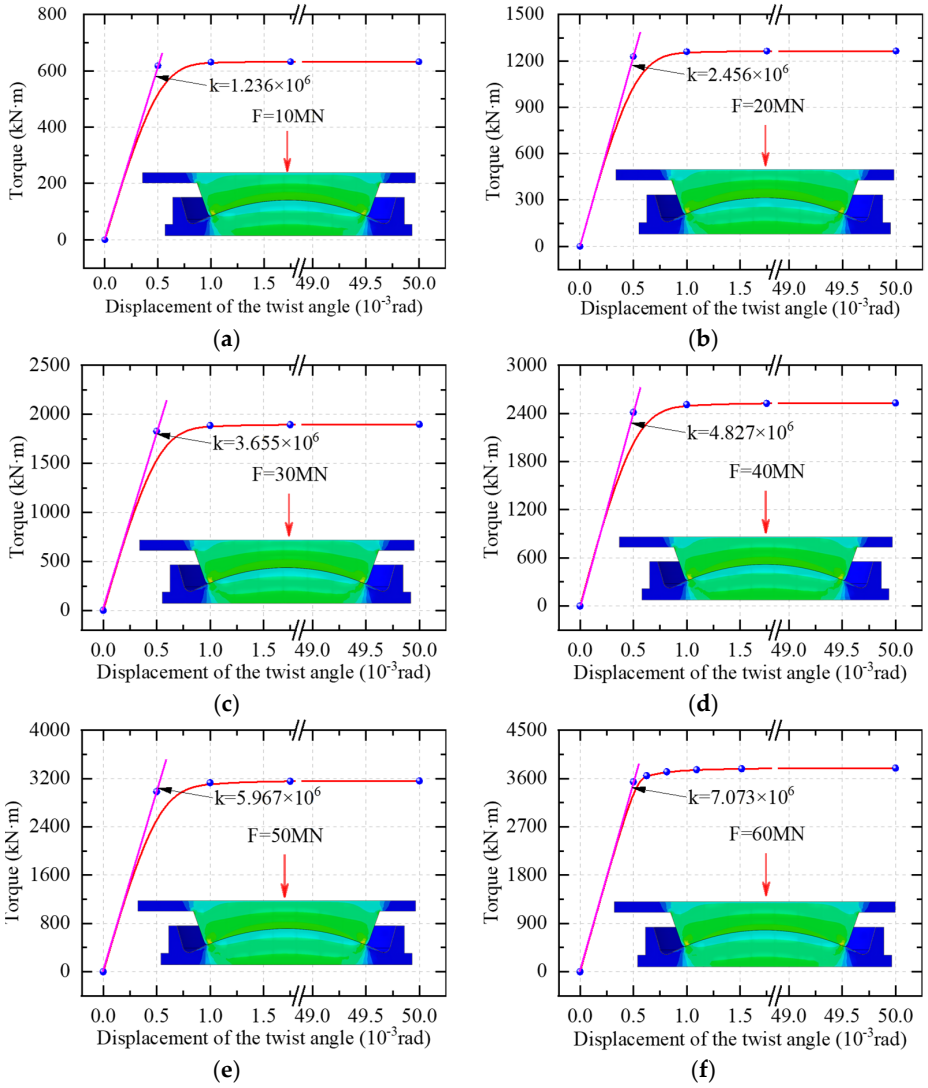

Figure 6. Load–displacement curve in six cases with different vertical forces: (**a**) the vertical force F = 10 MN; (**b**) the vertical force F = 20 MN; (**c**) the vertical force F = 30 MN; (**d**) the vertical force F = 40 MN; (**e**) the vertical force F = 50 MN; (**f**) the vertical force F = 60 MN.

According to the load–displacement curve in Figure 6, when the angle displacement increases sharply and the torque remains unchanged, the torque at this moment is considered as the critical torque. The comparison graph between the critical torque calculated using the FE method and that calculated by Equation (6) is shown in Figure 7. It can be seen from the figure that the difference between the two methods is within 5%, so the FE model can be considered correct and it can be employed to perform the RCS analysis of UHS.

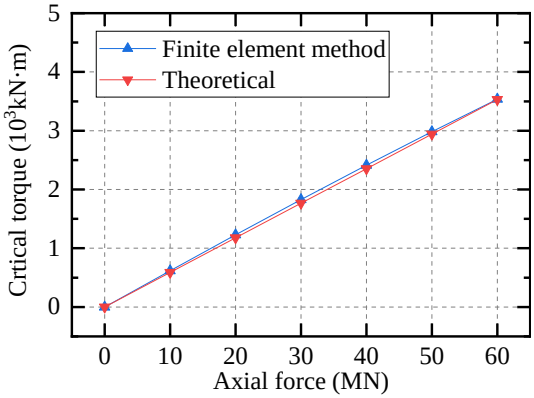

Figure 7. The critical torque obtained by the finite element method and theoretical calculation.

2. FE-based RCS Analysis

The slope of the linear rising segment of the above load–displacement curves is taken as the RCS of UHS, as shown in Figure 6. It can be seen from Figure 6a that when the vertical force is 10 MN, the slope of the linear rising segment takes the value of k = 123.609 kN·m/rad. Similarly, the RCS parameters under the vertical force of 20 MN, 30 MN, 40 MN, 50 MN, and 60 MN can be obtained from Figure 6b–f. Furthermore, the relationship between the RCS and vertical force can be obtained as shown in Figure 8.

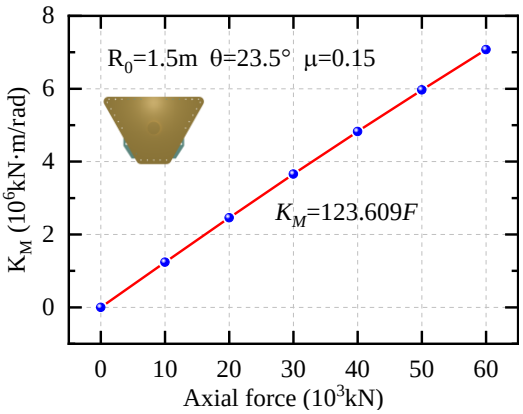

Figure 8. The rotational constraint stiffness of UHS.

Figure 8 shows that the RCS increases almost linearly with the increase in the vertical force of the bridge tower. Therefore, RCS can be calculated through the interpolation method according to the vertical force at each construction stage. The related curve of RCS and the vertical forces is fitted using the least square method in order to obtain the following expression equation:

$$K_M = 123.609F = \alpha \times F \quad (8)$$

where the unit of RCS K_M is kN·m/rad, and the unit of vertical force F is kN. α is a coefficient with dimensions measured in m/rad.

3.2.2. Influence of Central Angle on RCS

When the curvature radius R_0 = 1.5 m, friction coefficient μ = 0.15, and vertical force F = 10 MN, the rotational performances of UHS with central angles of 13°, 16.5°, 20°, 23.5°, and 27° were studied. The UHS responses are shown in Figures 9 and 10.

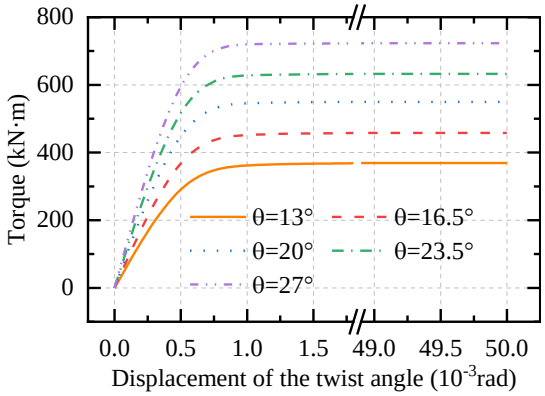

Figure 9. Torque–displacement curves with different central angles.

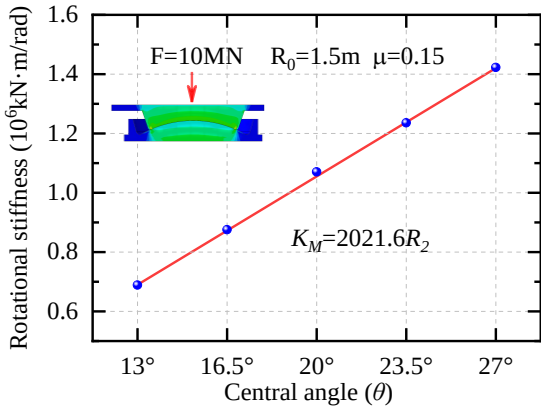

Figure 10. Related curve of the RCS-central angle.

Figure 9 shows that the critical torque increases with the increase in the central angle. According to the above method, RCS can be obtained as shown in Figure 10. It can be concluded that when the vertical force, radius of curvature, and friction coefficient have certain values, the RCS increases with the increase in the central angle by a linear trend.

As $R_2 = R_0 \times \theta \times \frac{\pi}{180^\circ}$, RCS has a positive proportional relationship with R_2. The related curve of RCS and the radius of the contact surface is fitted using the least square method in order to obtain the following expression equation:

$$K_M = 2021.6R_2 = \beta \times R_2 \quad (9)$$

where the unit of RCS K_M is kN·m/rad, and the unit of radius of arc-contact surface is mm. β is a coefficient with dimensions measured in kN/rad.

3.2.3. Influence of Curvature Radius of Contact Surface on RCS

The influence of the curvature radius of the contact surface on the RCS was studied with R_0 = 1.5 m and R_0 = ∞ (the contact surface is plane), under the premise of ensuring the same radius for the contact surface (R_2). The critical torques are shown in Figure 11 with different R_2 or R_0.

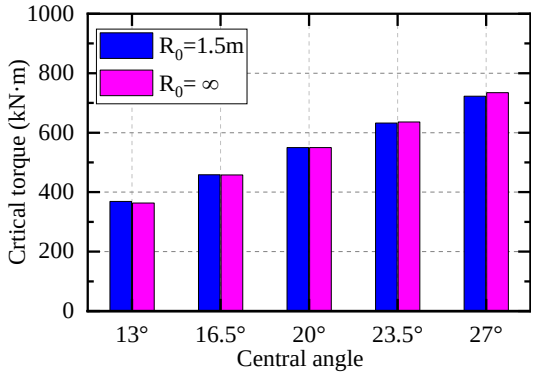

Figure 11. The critical torque under different R_2 or R_0.

Figure 11 shows that the difference between the critical torque was less than 5% with R_0 taking a different value. Thus, it can be concluded that R_2 and F must be unchanged. At this point, it can be considered that the rotational performance of UHS is independent of the radius of curvature.

3.2.4. Influence of Friction Coefficient of Contact Surface on RCS

The rotational performances of UHS were studied with friction coefficients of 0.03, 0.06, 0.09, 0.12, and 0.15. The curvature radius took the value of R_0 = 1.5 m, central angle, and vertical force F = 10 MN. The responses of UHS are shown in Figures 12 and 13.

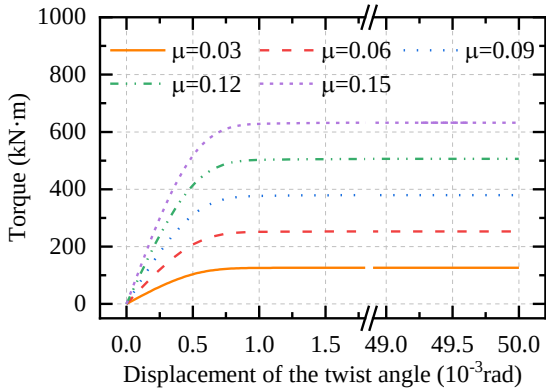

Figure 12. Torque–displacement curves under different friction coefficients.

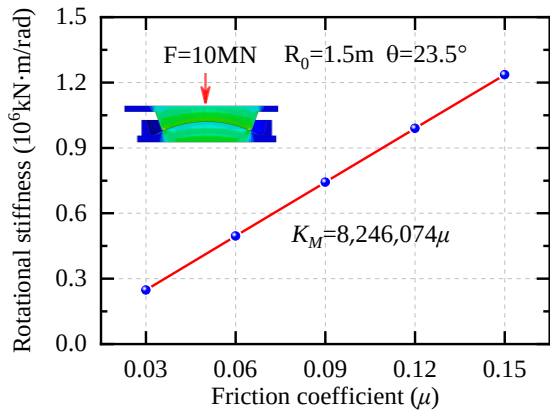

Figure 13. Variation curve of RCS with the friction coefficient.

Figure 12 shows that the critical torque increased with the increase in the friction coefficient. Similarly, the related curve of RCS-μ can be acquired, as shown in Figure 13.

It can be concluded that RCS increases with the increase in the friction coefficient in an approximate line when the vertical force, radius of curvature, and central angle are not changed.

The related curve of RCS and the friction coefficients is fitted using the least square method to obtain the following expression equation:

$$K_M = 8246074\mu = \gamma \times \mu \tag{10}$$

where the unit of RCS K_M is kN·m/rad, and γ is a coefficient with dimensions of (kN·m/rad).

3.3. RCS Calculation Model of UHS

In order to establish the calculation model of the RCS under the joint influence of multi-parameters, according to the influence law of each parameter (R_2, μ, F) on the RCS from Section 3.2, that is, RCS has a linear relationship with the radius of the contact surface, the friction coefficient of the contact surface, and the vertical force, respectively, the calculation model of the RCS with multi-parameters were obtained by coupling the three influence parameters into the initial model (Equations (8)–(10)), as shown in Equations (11)–(13):

$$K_M = \frac{123.609}{\mu \times R_2}\mu \times F \times R_2 = 1340\mu \times F \times R_2 = \xi_1 \times \mu \times F \times \theta \times R_0 \times \frac{\pi}{180^\circ} \tag{11}$$

$$K_M = \frac{2021.6}{\mu \times F}\mu \times F \times 1000R_2 = 1347.7\mu \times F \times R_2 == \xi_2 \times \mu \times F \times \theta \times R_0 \times \frac{\pi}{180^\circ} \tag{12}$$

$$K_M = \frac{8246074}{F \times R_2}\mu \times F \times R_2 = 1340.8\mu \times F \times R_2 = \xi_3 \times \mu \times F \times \theta \times R_0 \times \frac{\pi}{180^\circ} \tag{13}$$

It can be seen that the results of the three Equations (11)–(13) are very close to each other, which verifies that the modeling method of coupling multi-factors after univariate analysis is advisable. In order to unify the calculation models, take the average value calculated by Equations (11)–(13) as the calculation model of RCS:

$$K_M = \xi \times \mu \times F \times \theta \times R_0 \times \frac{\pi}{180^\circ} = \frac{\xi_1 + \xi_2 + \xi_3}{3} \times \mu \times F \times \theta \times R_0 \times \frac{\pi}{180^\circ} = 1342.8\mu \times F \times \theta \times R_0 \times \frac{\pi}{180^\circ} \tag{14}$$

where the unit of RCS K_M is kN·m/rad, and the unit of vertical force F is kN. Among them, ξ is a non-dimensional coefficient.

It should be noted that the radius of the arc-contact surface R_2 directly affects the RCS. Both the central angle θ and curvature radius R_0 jointly affect the arc-contact surface radius R_2, which indirectly affects the RCS. That is, when R_2 is constant, changing R_0 cannot affect the RCS. Therefore, Equation (14) can be finally written as:

$$K_M = 1342.8\mu \times F \times \theta \times R_2 \tag{15}$$

where $R_2 = R_0 \times \theta \times \frac{\pi}{180^\circ}$.

The friction coefficient μ in the model could be any value, which depends on the lubrication effect between the top plate and the bottom basin of the UHS. F could be the vertical force generated by different bridge structures or induced at the different construction. R_2 should be determined according to the geometric parameters of the contact surface between the top plate and the bottom basin of the UHS used in different structures. Therefore, this model is applicable to the calculation of the horizontal rotational stiffness of any structures using UHS.

In practical applications, the geometric parameters R_0 and θ can be easily obtained according to the design data, the friction coefficient μ is provided by the manufacturer, and the vertical force F can also be easily obtained at each stage according to the structural calculation. Therefore, the RCS can be easily obtained by Equation (15) in this study. Engineers input the calculated RCS into the mechanical model as a boundary parameter

in order to perform the mechanical calculation of the structure construction stage, and then the mechanical response of the whole structure can be obtained accurately and fast. This method avoids complicated modeling and calculation work, thus greatly reducing the calculation cost, contributing to the project by saving time and shortening the construction period and thus running smoothly.

To verify the accuracy of the proposed method in this paper, we compared the RCS calculation results of the proposed method with those of the finite element method for eight different groups of parameters, as shown in Table 1.

Table 1. Comparison between the proposed method and the finite element method.

Number	μ	R_0 (m)	θ (°)	F (kN)	Formula K_M (kN·m/rad)	FEM K_M (kN·m/rad)	Error (%)
1	0.05	1.5	23.5	30,000	1,054,098	1,059,650	0.5
2	0.05	1.5	23.5	50,000	1,756,830	1,728,214	−1.6
3	0.05	1.5	25	30,000	1,423,032	1,416,175	−0.5
4	0.05	1.5	25	50,000	2,371,721	2,336,819	−1.5
5	0.1	1.5	23.5	30,000	2,108,196	2,107,738	0.0
6	0.1	1.5	23.5	50,000	3,513,660	3,422,899	−2.6
7	0.1	1.5	25	30,000	2,846,065	2,825,381	−0.7
8	0.1	1.5	25	50,000	4,743,441	4,653,838	−1.9

Table 1 shows that the maximum error of the calculation results between the proposed method in this paper and the FE-based method is 2.6%, which can meet the calculational accuracy of engineering.

4. Calculation Procedure of Mechanical Properties of Cable-Stayed Bridge with UHS

UHS is used to connect the bridge tower and pier when the transverse direction of the cable-stayed bridge is asymmetric, and the mechanical properties of the cable-stayed bridge structure can be calculated according to the flow framework shown in Figure 14.

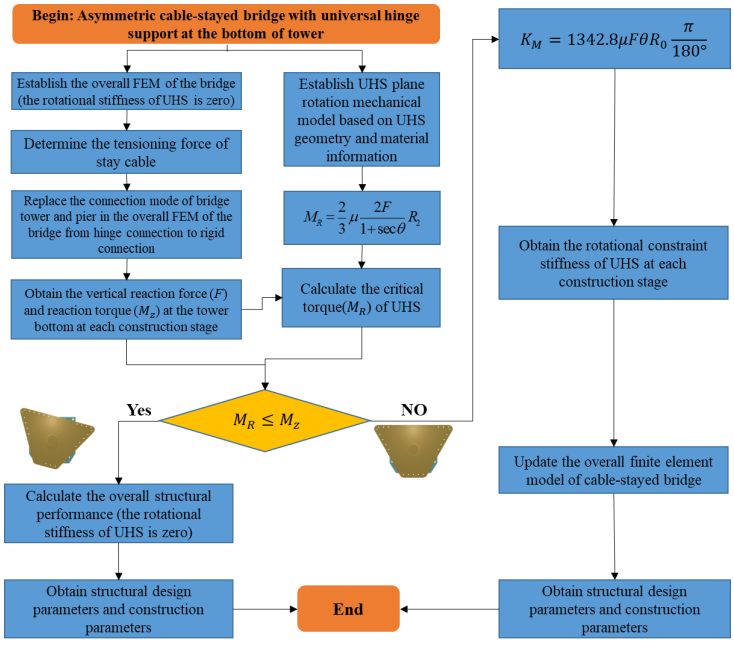

Figure 14. Calculation procedure of the cable-stayed bridge with UHS.

5. Case Study: An Inclined Single-Tower Cable-Stayed Bridge

An actual bridge project was studied to further verify the correctness of the proposed calculation formula for RCS in this paper, and to learn the importance of RCS to the structural response.

5.1. Bridge Overview

The Sanya Landscape Bridge is a special-shaped inclined single-tower cable-stayed bridge that uses UHS in the support of the bridge tower for the first time. The design idea of this bridge is a mast with a sightseeing platform (Cloud Ring) as the bridge tower. The Cloud Ring not presents a trendy and fashionable city image of Sanya in China for citizens and tourists, but also has the meaning of eternity and being everlasting, which gives a strong romantic feel to the bridge. The landscape design rendering of the bridge is shown in Figure 15. The total length of the bridge is 233.4 m (length of steel deck), and the bridge span is arranged as 99.8 m + 51.0 m + 25.0 m + 27.4 m + 30.2 m.

Figure 15. The Sanya Landscape Bridge.

The main beam is a double-sided I-shaped steel beam, which presents a "Y" shaped asymmetric curve widening shape on the plane, and the beam width is 7.2–11.7 m, with a main beam height of 0.88 m. The bridge tower is a steel inclined single tower with a trapezoidal section, and has a shuttle shape. Its length is 85 m with an inclination of 60°. The viewing platform is set away from the bottom of the tower, 50 m in a vertical direction.

The cable-stayed bridge is equipped with the south rear ground anchor cable (S1~S4), the north rear ground anchor cable (N1~N4), the front ground anchor cable (Q1~Q4), the south main beam cable (B1-S~B9-S), the north main beam cable (B1-N~B9-N), and the rhombic cable (Y1~Y6). The three-dimensional model and details of the components of the bridge are shown in Figure 16.

Q420 steel is used for the main beam and bridge tower, and Q345 steel is used for the pier below the main beam. The rear ground anchor cables adopt strands with a tensile strength not less than 1860 MPa, and the other stayed cables adopt a parallel steel wire with 1670 MPa tensile strength. The construction process of the bridge is divided into 16 stages, and the specifics are shown in Table 2.

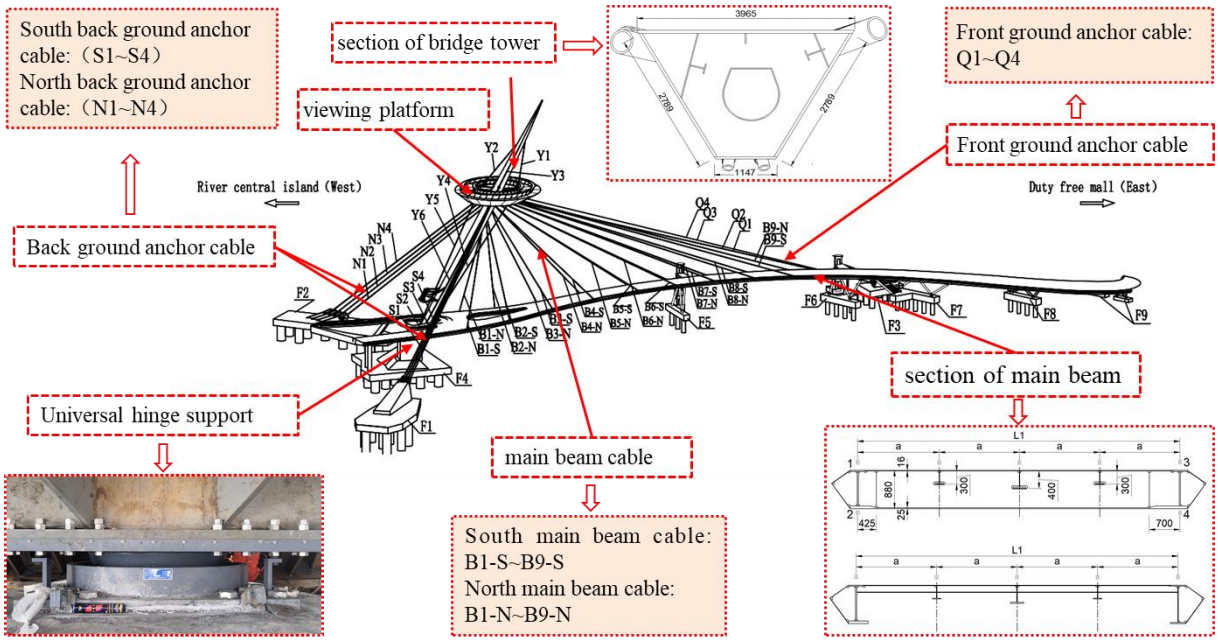

Figure 16. Schematic diagram of the Sanya Landscape Bridge (unit: mm).

Table 2. Construction steps.

Stages	Contents of Construction Stage
stage1	Vertical rotation of bridge tower in place
stage2	Tensioning ground anchor cables N1, S1, Q1~Q4
stage3	Tensioning ground anchor cables N2, S2
stage4	Tensioning ground anchor cables N3, S3
stage5	Tensioning ground anchor cables N4, S4
stage6	Tensioning main beam cable B1
stage7	Tensioning main beam cable B9
stage8	Tensioning main beam cable B2
stage9	Tensioning main beam cable B8
stage10	Tensioning main beam cable B3
stage11	Tensioning main beam cable B7
stage12	Tensioning main beam cable B4
stage13	Tensioning main beam cable B6
stage14	Tensioning main beam cable B5
stage15	Second tensioning ground anchor cables Q2, Q3
stage16	Second tensioning ground anchor cables Q1, Q4

5.2. Finite Element Model of the Cable-Stayed Bridge

The finite element software Midas/civil is used to establish the space grillage analysis model, which lays the foundation for the subsequent analysis of RCS. The beam element is employed to simulate the bridge tower, main beam, and pier, and the stay cable is simulated by a truss element and nonlinear cable element. Elastic connection is used between the bridge tower and pier to the limit translational constraint and release rotational constraint. The end of the beam adopts fixed constraints. The main beam and the pier are hinged, and the general connection in the elastic connection is adopted to restrict the translation and release the rotation. The FE model of the whole bridge is shown in Figure 17.

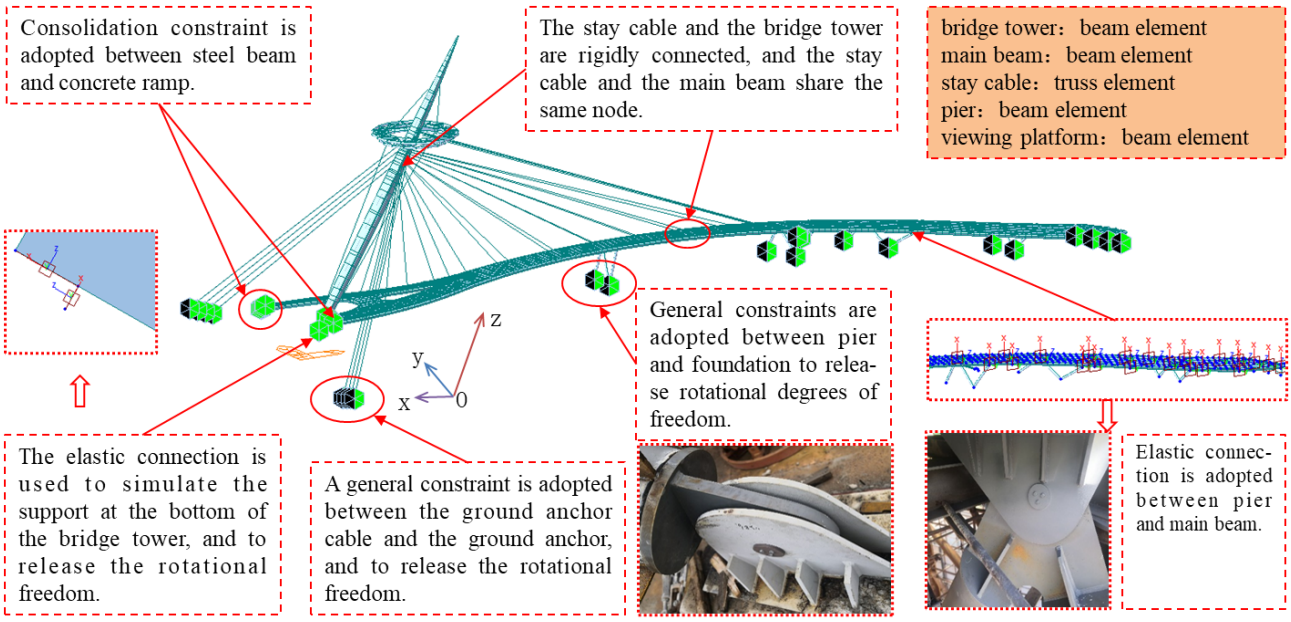

Figure 17. Integral finite element model of the cable-stayed bridge.

5.3. Calculation of RCS at Each Construction Stage

Replace the hinge constraint at the bottom of the tower with a fixed constraint in the overall analysis model of the bridge, keep the tension of the stayed cable unchanged, and perform the forward analysis to obtain the reaction force at the bottom of the tower at each construction stage (these details are shown in Table 3). The direction of the coordinate axis can be determined by referring to Figure 17. The maximum value of the vertical force occurs in the final construction stage (stage16) takes a value of 51,157 kN. The maximum reaction torque at the bottom of the tower occurs in the completion stage of the tensioning of the main beam cable (stage14), and takes a value of 1384 kN·m.

Table 3. Reaction force of the tower bottom at each construction stage.

Construction Step	Vertical Force Fz /kN	Reaction Torque Mz /kN·m	Construction Step	Vertical Force Fz /kN	Reaction Torque Mz /kN·m
Stage1	5590	9	Stage9	47,712	1066
Stage2	16,253	5	Stage10	48,504	1202
Stage3	25,270	65	Stage11	49,305	1269
Stage4	32,675	220	Stage12	50,002	1318
Stage5	38,161	526	Stage13	50,335	1337
Stage6	40,701	199	Stage14	51,000	1384
Stage7	44,476	439	Stage15	51,076	645
Stage8	46,034	862	Stage16	51,157	171

In this case, the friction coefficient of UHS was provided by the manufacturer, which is $\mu = 0.15$. The curvature radius of the contact surface is $R_0 = 1.5$ m and the central angle is $\theta = 23.5°$.

The reaction torque under each vertical force (in Table 2) is compared with the critical torque calculated by Equation (6) for the corresponding vertical force, and the comparison results are shown in Figure 18. The results show that the torque of the actual construction stage was less than the critical torque. It can be concluded that UHS is always in the state of static friction during the whole construction process because of the existence of the friction between the top plate and the bottom basin. Therefore, UHS cannot be simulated according to the ideal hinge support, and its actual rotational parameters (RCS) should be calculated according to Equation (15).

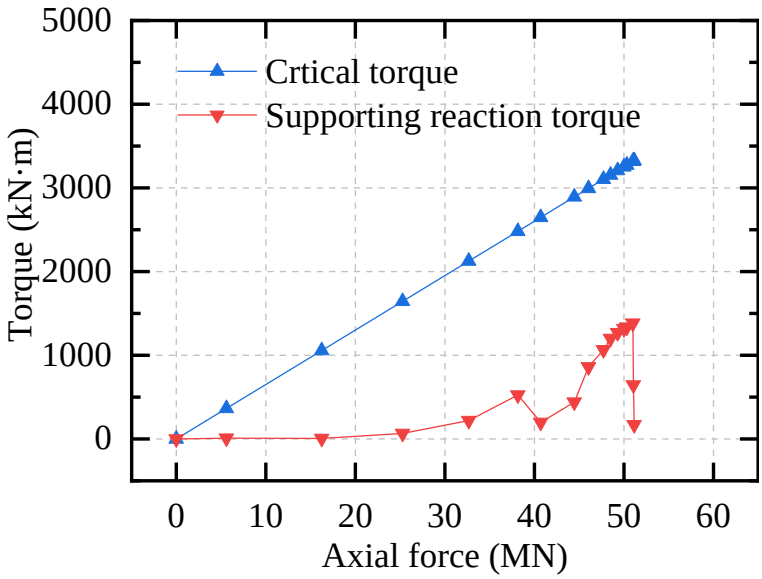

Figure 18. The critical torque and reaction torque under various conditions.

5.4. Verification of RCS Calculation Model Based on Monitoring Data

The deformation along the longitudinal direction of the viewing platform is used to reflect the rotational displacement of the bridge tower to more clearly exhibit the rotational effect of the bridge tower. Reference point 1 (RP1) and reference point 2 (RP2) are set on the viewing platform, and are employed as the monitoring points for the rotation displacement of the bridge tower during the construction process, as shown in Figure 19.

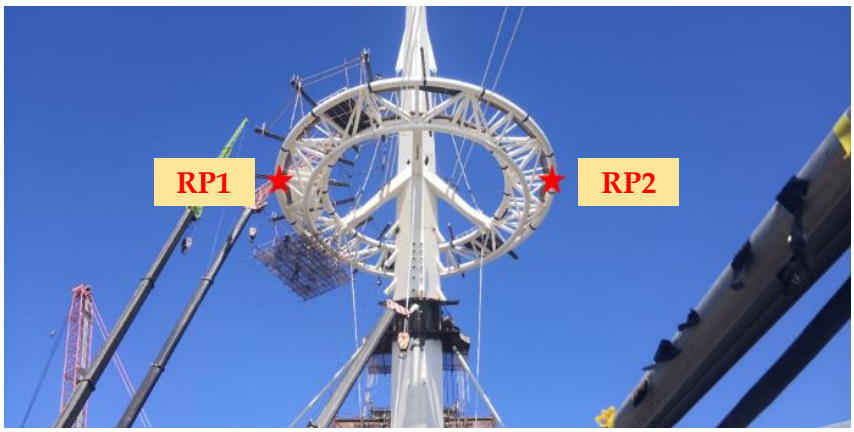

Figure 19. Layout of monitoring points.

Two FE models considering the RCS of the UHS (the rotational restraint stiffness calculated from Equation (15)) and without considering the RCS of the UHS (the rotational stiffness is zero) are established, respectively, both of them include the entire construction process. The influence of the RCS on the attitude of the bridge tower in each construction stage is analyzed. The same tension is applied to the two models, respectively, and the bridge tower states at each construction stage are obtained. A comparison of the rotation angle of the bridge tower in each construction stage of the two models is shown in Figure 20.

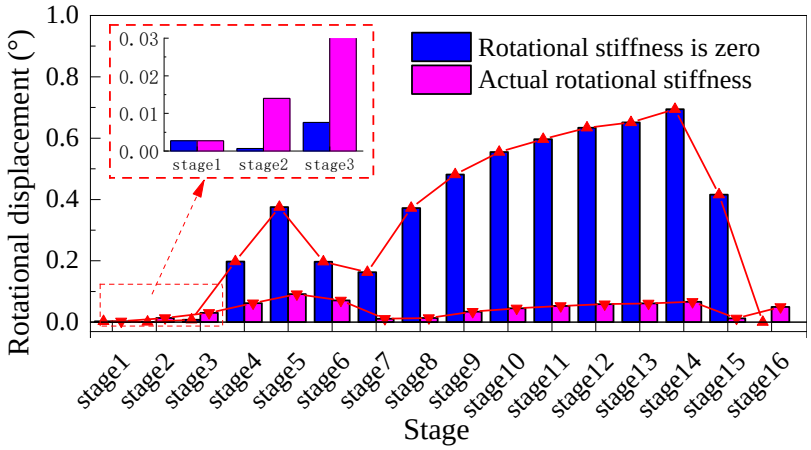

Figure 20. Comparison of the rotation displacement of the bridge tower.

Figure 20 shows that whether the RCS is considered or not will make a significant difference when designing the bridge tower during construction. The maximum difference occurs at stage 14, which is reflected by the maximum difference of the displacement at the monitoring point along the longitudinal direction of the bridge, which is about 265 mm, and this error is unacceptable for construction. If the inducement of the error caused by the failure to consider the RCS is not learned for engineers, it may mislead engineers into thinking about other induction factors, further leading to a wrong decision. Therefore, it is significant for accurately obtaining the rotational displacement of the tower to take into account the RCS at each construction stage.

Readjust the tension of the cable according to the calculated RCS, analyze and calculate the deformation of the bridge tower at each construction stage, and compare it with the measured value, as shown in Figure 21.

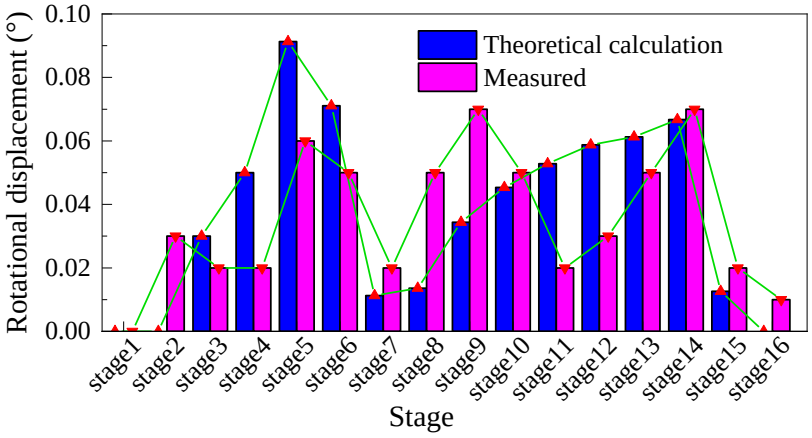

Figure 21. Comparison between theoretical and measured rotation angle of bridge tower.

Figure 21 shows that the maximum difference between the theoretical rotation angle and the measured one occurs at stage 8 (tensioning the main beam cable B2), where its value is 0.04°. This equates to about 15 mm through the displacement of the monitoring point along the longitudinal direction, and this error is acceptable in engineering. Analyze the reasons for the errors, which may be caused by a long measuring distance, systematic error of the measuring instrument, etc. In addition, compared with the condition that does not consider RCS, the error of the measured and calculated rotational displacements is reduced by about 90%. Therefore, the proposed method in this paper is a great approach to effectively calculate the RCS in practical applications.

6. Discussion

The proposed model in this study is a fast calculation method for the rotational constraint stiffness, which greatly reduces the calculation cost and saves time. Although there are some errors in the calculation results, the precision has been greatly improved compared with the traditional structure analysis method that does not consider the work of this paper, and the errors are completely acceptable in engineering. For a transverse symmetric bridge, the rotation behavior of the UHS in the horizontal plane can be ignored when the cable force error satisfies the construction accuracy. Therefore, this study mainly focuses on the transverse asymmetric cable-stayed bridges. In the implementation of the case in this paper, it was found that the measured displacements in the transverse and longitudinal directions were almost consistent with the theoretical displacements calculated according to the ideal hinge support, while the rotation angles of the bridge towers in the horizontal plane are quite different from it, so the rotational behavior of the UHS in the horizontal plane is considered as being important in this study. More practical case studies should be performed to further explore the practicability of the proposed method and to comprehensively evaluate the mechanical properties of UHS in the future.

7. Conclusions

(1) To improve the efficiency and accuracy of the mechanical analysis procedure of the cable-stayed bridge with UHS, a calculation method for the rotational constraint stiffness of UHS is proposed. The rotational constraint stiffness obtained by the proposed method is used to modify the boundary parameters of the whole calculation model to calculate the mechanical properties of the whole structure quickly.

(2) The proposed method takes into account the geometry, material parameters, and the load factors of UHS, so it has a strong applicability for all kinds of cable-stayed bridges with UHS.

(3) The proposed method was applied to a practical case to verify the effectiveness, and the results show that the method can greatly reduce the calculation error, shorten the calculation time, save the calculation cost, and effectively speed up construction, so it is especially suitable for the whole process of structure analysis.

Author Contributions: Y.Z. (Yajun Zhang): conceptualization, methodology, software, formal analysis, investigation, and writing—original draft. Y.Z. (Yu Zhao): conceptualization, methodology, supervision, and project administration. Y.Z. (Yongjun Zhou): methodology, writing—review and editing, and supervision. X.Y.: software, validation, formal analysis, writing—review and editing, and visualization. All authors have read and agreed to the published version of the manuscript.

Funding: This research was funded by Natural Science Foundation Project of Shaanxi China (No. 2021JLM-47) and Key Research and Development Program of Ningxia Hui Autonomous Region (No. 2022BEG03062).

Institutional Review Board Statement: Not applicable.

Informed Consent Statement: Not applicable.

Data Availability Statement: The data used to support the findings of this study are available from the corresponding author upon request.

Acknowledgments: This research was funded by the Natural Science Foundation Project of Shaanxi China (No. 2021JLM-47) and Key Research and Development Program of Ningxia Hui Autonomous Region (No.2022BEG03062), and this support is gratefully acknowledged. In addition, the authors would like to thank Yingxin Hui from Ningxia Communications Construction Co., Ltd., for his guidance with the numerical model.

Conflicts of Interest: The authors declare no conflict of interest.

Nomenclature

STCSB	single-tower cable-stayed bridge
UHS	universal hinge support
RCS	rotational constraint stiffness
FE	finite element
F	vertical force transferred from tower to UHS
M	reaction torque
M_R	critical torque
R_0	spherical radius of UHS
R_1	radius of the vertical projection surface of the arc-contact surface
R_2	radius of the arc-contact surface
θ	central angle
q_0	uniform distributed force at the top plate
q	uniform distributed force at the bottom basin
q_v	vertical component force of q
q_t	tangential component force of q in the arc surface
f	friction force
r	radius of the micro-ring
ds	area of the micro-ring
μ	friction coefficient
k	slope of the load-displacement curve
K_M	rotational constraint stiffness of the UHS
α	a coefficient with dimensions (m/rad)
β	a coefficient with dimensions (kN/rad)
γ	a coefficient with dimensions (kN·m/rad)
ξ	a dimensionless coefficient

References

1. Podolny, W.; Scalzi, J.B. *Construction and Design of Cable-Stayed Bridges*, 2nd ed.; Wiley: New York, NY, USA, 1986.
2. Troitsky, M.S. *Cable-Stayed Bridges: Theory and Design*; Crosby Lockwood Staples: London, UK, 1977.
3. Shilin, L.; Liang, Z.; Meng, F. *Cable Stayed Bridge*; China Communications Press: Beijing, China, 2002. (In Chinese)
4. Watson, C.; Watson, T.; Coleman, R. Structural Monitoring of Cable-Stayed Bridge: Analysis of GPS versus Modeled Deflections. *J. Surv. Eng.* **2007**, *133*, 23–28. [CrossRef]
5. Guest, J.K.; Draper, P.; Billington, D.P. Santiago Calatrava's Alamillo Bridge and the Idea of the Structural Engineer as Artist. *J. Bridge Eng.* **2013**, *18*, 936–945. [CrossRef]
6. Aparicio, A.C.; Casas, J.R.; Calatrava, S. The Alamillo Cable-Stayed Bridge: Special Issues Faced in The Analysis and Construction. Proceedings of the Institution of Civil Engineers. *Struct. Build.* **1997**, *122*, 432–450. [CrossRef]
7. Casas, J.R.; Aparicio, A.C. Monitoring of The Alamillo Cable-Stayed Bridge During Construction. *Exp. Mech.* **1998**, *38*, 24–28. [CrossRef]
8. Fernandez Troyano, L.; Manterola Armisen, J. Bridge over the River Lerez, In Pontevedra. Reflection on The Waters. *Cauce* **1995**, *2000*, 60–67.
9. Liu, Y.-J.; Zhou, X.-H.; Yan, D.-H.; Geng, J. Stress analysis of tower-beam joint of inclined tower cable-stayed bridge with steel-concrete girder. *China J. Highway Transp.* **2003**, 66–70. [CrossRef]
10. Troyano, L.F.; Armisén, J.M.; Suárez, M.A.A. The Inclined Towers of the Ebro and Lérez Bridges. *Struct. Eng. Int.* **1998**, *8*, 258–260. [CrossRef]
11. Chvojková, P.N.; Fošumpaur, P.; Hladík, M.; Horský, M.; Kašpar, T.; Králík, M.; Zukal, M. Historical and Modern Bridges over the Elbe-Vltava Waterway. In *IOP Conference Series: Materials Science and Engineering*; IOP Publishing: Bristol, UK, 2021; Volume 1203, p. 022014.
12. Zhang, Y.; Wang, X.; Liu, Y.; Li, R. Study on Boundary Conditions of Ground Anchored Cable Stayed Bridge with Single Inclined Tower. In *IOP Conference Series: Earth and Environmental Science*; IOP Publishing: Bristol, UK, 2021; Volume 647, p. 012026.
13. Martins, A.M.; Simões, L.M.; Negrão, J.H. Optimization of cable-stayed bridges: A literature survey. *Adv. Eng. Softw.* **2020**, *149*, 102829. [CrossRef]
14. Yan, Y.-H.; Sun, Y.-G.; He, L.-Z. Construction Control of New Tuanbo Bridge in Tianjin. *Bridge Constr.* **2013**, *43*, 99–103. (In Chinese)
15. Wang, S. Study on Cable Tension Method of Spatial Cable Plane. *Munic. Technol.* **2016**, *34*, 53–56. (In Chinese)
16. Song, J. Construction technology of color needle steel single tower for long span cable-stayed bridge. *Natl. Def. Transp. Eng. Technol.* **2019**, *17*, 36–39+30. (In Chinese)

17. Hou, M.; Zhang, Z.-Q.; Fan, Z.-W. Overall Design of Haitang Bay Cable-Stayed Pedestrian Bridge in Sanya. *World Bridges* **2021**, *49*, 1–6. (In Chinese)
18. Zhou, Y.; Tian, R.; Wu, L.; Zhao, Y. Mechanical characteristics analysis of pylon-hinged single-pylon cable-stayed bridge during construction. *Sci. Technol. Eng.* **2020**, *20*, 8785–8790. (In Chinese)
19. Amer, T.S.; Galal, A.A.; Abady, I.M.; Elkafly, H.F. The dynamical motion of a gyrostat for the irrational frequency case. *Appl. Math. Model.* **2021**, *89*, 1235–1267. [CrossRef]
20. Amer, W.S. Modelling and analyzing the rotatory motion of a symmetric gyrostat subjected to a Newtonian and magnetic fields. *Results Phys.* **2021**, *24*, 104102. [CrossRef]
21. Li, J.Z.; Peng, T.B.; Xu, Y. Damage investigation of gird-er bridges under Wenchuan Earthquake and corresponding seismic design recommendations. *Earthq. Eng. Eng. Vib.* **2008**, *7*, 337–344. [CrossRef]
22. Itoh, Y.; Yazawa, A.; Kitagawa, T.; Kainuma, S.; Yamamoto, Y.; Kutsuna, Y. Study on environmental durability of rubber bearing for bridges. In *IABSE Symposium Report International Association for Bridge and Structural Engineering*; Currant Associates Inc.: New York, NY, USA, 2002.
23. Gu, H.S.; Itoh, Y. Ageing behaviors of natural rubber and high damping rubber materials used in bridge Rubber bearings. *Adv. Struct. Eng.* **2010**, *6*, 1105–1113. [CrossRef]
24. Itoh, Y.; Gu, H.; Satoh, K.; Kutsuna, Y. Experimental investigation on ageing behaviors of rubbers used for bridge bearings. *Struct. Eng./Earthq. Eng.* **2006**, *62*, 17–31. [CrossRef]
25. Fogato, M. The role of boundary conditions in the torsional instability of suspension bridges. *J. Math. Anal. Appl.* **2023**, *518*, 126729. [CrossRef]
26. Adema, A.; María, H.S.; Guindos, P. Analysis of instant and long-term performance of timber-concrete floors with boundary conditions other than simply supported. *Eng. Struct.* **2022**, *254*, 113827. [CrossRef]
27. Han, Q.; Zhang, Y.-G.; Zhao, K.-H. A Numerical Method of the Contact Problems in Structural Engineering. *J. Beijing Univ. Technol.* **2006**, *4*, 321–326. (In Chinese)
28. Guo, X.-M.; Zhao, H.-L. Study on contact problems in engineering structures. *J. Southeast Univ. (Nat. Sci. Ed.)* **2003**, *5*, 577–582. (In Chinese)
29. Fang, X.; Zhang, C.; Chen, X.; Wang, Y.; Tan, Y. A new universal approximate model for conformal contact and non-conformal contact of spherical surfaces. *Acta Mech.* **2014**, *226*, 1657–1672. [CrossRef]
30. Li, Z.X.; Zhou, T.Q.; Chan, T.H.T.; Yu, Y. Multi-scale numerical analysis on dynamic response and local damage in long-span bridges. *Eng. Struct.* **2007**, *29*, 1507–1524. [CrossRef]
31. Zhou, M.; Ning, X.; Nie, J. 4-D multiscale finite element analysis of the hybrid zone for cable-stayed bridges with steel-concrete hybrid girders. *J. Tsinghua Univ. (Sci. Technol.)* **2014**, *54*, 1321–1326.
32. Wang, Y.; Li, Z.; Wang, C.; Wang, H. Concurrent multi-scale modelling and updating of long-span bridges using a multi-objective optimisation technique. *Struct. Infrastruct. Eng.* **2013**, *9*, 1251–1266. [CrossRef]
33. Xiao, X.; Yan, Y.; He, J.; Chen, B. Multi-scale finite element modeling and model updating of long span cable-stayed bridge. *J. Huazhong Univ. Sci. Technol. (Nat. Sci. Ed.)* **2017**, *45*, 121–127.
34. Zheng, L.; Wang, W.-D. Multi-scale numerical simulation analysis of CFST column-composite beam frame under a column-loss scenario. *J. Constr. Steel Res.* **2022**, *190*, 107151. [CrossRef]
35. Wang, W.; Li, H.; Wang, J. Progressive Collapse Analysis of Concrete-filled Steel Tubular Column to Steel Beam Connections Using Multi-scale Model. *Structures* **2016**, *9*, 123–133. [CrossRef]
36. Salehi, M.; Erduran, E. Identification of boundary conditions of railway bridges using artificial neural networks. *J. Civ. Struct. Heal. Monit.* **2022**, *12*, 1223–1246. [CrossRef]
37. Li, B.; Wang, S.-H.; Yan, Q.-M. Rotational Performance and Structural Analysis of Spherical Bearing Based on ABAQUS Nonlinear Contact Analysis. *Railw. Eng.* **2012**, *11*, 10–13. (In Chinese)
38. Peng, T.-B.; Shi, X.-F. Theoretical Study of a Simplified Formula for Rotating Torque of Spherical Bearings. *Bridge Constr.* **2014**, *44*, 92–97. (In Chinese)
39. Yang, F. Analysis of Basic Mechanical Performances Test Results for Spherical Bearings of Railway Bridge. *Railw. Eng.* **2021**, *61*, 23–26. (In Chinese)
40. Shi, K.-R.; Pan, W.-Z.; Jiang, Z.-R.; Lü, J.-F.; Luo, B. Mechanical Behaviors of Large-tonnage Complex Steel Spherical Hinged Support: Rotation Behavior Subjected to Axial Compressive Load. *J. South China Univ. Technol. (Nat. Sci. Ed.)* **2019**, *47*, 9–15. (In Chinese)